Loughborough University

This item was submitted to Loughborough's Institutional Repository (https://dspace.lboro.ac.uk/) by the author and is made available under the following Creative Commons Licence conditions.

creative commons

COMMONS DEED

**Attribution-NonCommercial-NoDerivs 2.5**

**You are free:**

- to copy, distribute, display, and perform the work

**Under the following conditions:**


**Attribution**. You must attribute the work in the manner specified by the author or licensor.

**Noncommercial**. You may not use this work for commercial purposes.

**No Derivative Works**. You may not alter, transform, or build upon this work.

- For any reuse or distribution, you must make clear to others the license terms of this work.
- Any of these conditions can be waived if you get permission from the copyright holder.

**Your fair use and other rights are in no way affected by the above.**

This is a human-readable summary of the Legal Code (the full license).

Disclaimer

For the full text of this licence, please go to:
http://creativecommons.org/licenses/by-nc-nd/2.5/

# Optimal Seed Recipe Design for Crystal Size Distribution Control for Batch Cooling Crystallisation Processes

E. Aamir, Z. K. Nagy*, and C.D. Rielly
Loughborough University, Loughborough, Leicestershire, LE11 3TU, United Kingdom;
*z.k.nagy@lboro.ac.uk

*The paper presents a novel quality-by-design framework for the design of optimal seed recipes for batch cooling crystallisation systems with the aim to produce a desired target crystal size distribution (CSD) of the product. The approach is based on a population balance model-based optimal control framework, which optimizes the compositions of seed blends, based on seed fractions that result from standard sieve analysis. The population balance model is solved using a combined quadrature method of moments and method of characteristics (QMOM-MOCH) approach for the generic case of apparent size-dependent growth. Seed mixtures are represented as a sum of Gaussian distributions, where each Gaussian corresponds to the seed distribution in a particular sieve size range. The proposed methods are exemplified for the model system of potassium dichromate in water, for which the apparent size-dependent growth kinetic parameters have been identified from laboratory experiments. The paper also illustrates the simultaneous application of in situ process analytical tools, such as focused beam reflectance measurement (FBRM) for nucleation detection, attenuated total reflection (ATR) UV/Vis spectroscopy for concentration monitoring, as well as the in-line use of laser diffraction particle sizing for real-time CSD measurement.*

## 1. Introduction

Crystallisation is a widely used separation technique for solid-liquid mixtures due to its ability to provide high purity products. Crystallisation processes have a wide range of application as a separation technique in many chemical, petrochemical, food, pharmaceutical and microelectronics industries (Abbott, 2001; Mangin et al., 2006; Middlebrooks, 2001; Olesberg et al., 2000; Shi et al., 2005; Wiencek, 2002). Although crystallisation is often used when the end product is required in crystalline form (Braatz, 2002; Hounslow and Reynolds, 2006), the process development and scale-up is not straightforward. Researchers generally spend considerable time and effort for the development of batch crystallisation processes for the production of crystalline compounds with consistent crystal properties i.e. purity, shape, size, habit, morphology, and size distribution. The shape of the crystal size distribution (CSD) of the product obtained from the crystallisation process strongly affects the efficiency of downstream operations such as filtration, drying and washing (Chung et al., 2000; Mullin, 2001; Wibowo et al., 2001), but may also have considerable impact on the bioavailability of

* Corresponding author: email: z.k.nagy@lboro.ac.uk (Z K Nagy), Tel:+44 1509 222516; Fax:+44 1509 223923

the active pharmaceutical ingredient (API). Most of the product properties (e.g. dissolution rate, bulk density, flow-ability, packing properties, etc.) are also directly related to the crystal size distribution (Chung et al., 2000). Although some of these properties can be related to the moments of the CSD, knowing and predicting the entire shape of the distribution allows the design and adaptation of operating policies to achieve improved product quality, and to accomplish novel quality-by-design (QbD) procedures.

The main difficulty in batch crystallisation is to produce a uniform and reproducible CSD (Braatz, 2002; Wibowo and Ng, 2001), which has been addressed by several approaches proposed in the literature. One way to enhance the control of CSD is to use supersaturation control (SSC) (Aamir et al., 2009a; Braatz, 2002; Doki et al., 2004; Fujiwara et al., 2005; Liotta and Sabesan, 2004; Nagy et al., 2008; Yu et al., 2006) or direct nucleation control (Abu Bakar et al., 2009a, 2009b; Woo et al., 2009), which drives the process within the metastable zone to avoid nucleation, or to generate controlled nucleation/dissolution events, respectively. Although these approaches can provide improved consistency of the CSD, they do not address the actual design of the CSD. The prediction and estimation of the shape of the distribution at the end of the batch can provide useful information for monitoring or designing the operating curve for the supersaturation controller. Model-based approaches can be used for better predictive control (Chung et al., 1999; Fujiwara et al., 2005; Larsen et al., 2006; Rawlings et al., 1993; Ward et al., 2006; Worlitschek and Mazzotti, 2004; Zhang and Rohani, 2003, Grosso et al., 2009) but also for product design by reverse engineering the process to achieve the desired CSD (Hounslow and Reynolds, 2006). Although these approaches have been proved to produce high quality crystals, in the vast majority of cases they do not take into account the characteristics of the seed.

Seeding has been known for a long time as an effective technique to stabilize batch crystallisation processes. In seeded crystallisation, ideally the supersaturation is maintained at the desired constant value throughout the entire batch by the application of properly designed control algorithms (Chung et al., 1999; Nagy and Braatz, 2003; Xie et al., 2001; Zhang and Rohani, 2003; Simon et al., 2009a). Supersaturation, generated by cooling, can be consumed by the growth of seeds added, and hence, it can be kept relatively low throughout the batch if enough seeds are loaded. Consequently, secondary nucleation can be avoided and the process can be stabilized. However, in practice in most of the cases the suppression of secondary nucleation is achieved by very conservative operation under the condition of slow cooling. In addition, quantitative information on the quality and property of seeds are seldom considered in the control of the process, and variations in seed CSD and property are generally considered as uncertainties rather than actuators for the control of the final CSD. Seeding seems to be treated as an art rather than science (Adi et al., 2007; Jagadesh et al., 1999; Kalbasenka et al., 2007; Kubota et al., 2001; Ludwick and Henderson, 1968; Lung-Somarriba et al., 2004) and

generally there is a lack of systematic methodologies related to the amount and size of seeds that should be added into a crystallizer to obtain a product with a desired size distribution. Although it is recognized that the most important manipulated variables for the optimisation of crystallisation processes are supersaturation trajectories as well as the seed characteristics (Bohlin and Rasmuson, 1996; Heffels and Kind, 1999; Kalbasenka et al., 2007; Ruf et al., 2000, Yannick et al., 2009), the number of approaches focusing on temperature or anti-solvent addition trajectory optimisations is disproportionally higher than contributions considering seed recipe optimisations. The approaches proposed so far, mainly consider the optimisation of the width and amount of a particular mono-modal seed distribution (Chung et al., 1999; Kalbasenka et al., 2007).

The paper presents a novel approach for the optimal seed recipe design for crystallisation processes according to which a target CSD with a desired shape may be obtained by blending different mixtures of seeds obtained from a standard sieving separation. The optimal seed recipe is obtained by solving a constrained non-linear optimization problem with the objective to achieve a desired shape of the CSD at the end of the batch, while operating within equipment and operational constraints (e.g. fixed temperature profile). The population balance model is solved using a combined quadrature method of moments and method of characteristics (QMOM-MOCH) approach (Aamir et al., 2009b), which provides a computationally efficient solution method for model-based optimisation. One of the novelties of the proposed method is that the optimisation will automatically select between existing seed fractions which practically would result from standard sieve analyses, and simultaneously determines the amount and sieve fractions (with fixed CSD), which need to be mixed to produce the seed. Hence the proposed approach provides a practical framework for seed recipe design.

In addition to the simulation results, according to the authors' knowledge the paper is one of the first contributions to provide experimental validation of the seed recipe design concept, using a specially designed laboratory setup, which includes *in situ* process analytical tools, such as focused beam reflectance measurement (FBRM), attenuated total reflectance (ATR) UV/Vis spectroscopy, as well as in-line CSD measurement using laser diffraction (Malvern Mastersizer). Extension to the approach could be developed using alternative CSD measurement approaches, based on in-line image analysis or using the recently developed internal or external Bulk Video Imaging (BVI) approaches (Simon et al., 2009b; 2009c). The optimal seed recipes are designed for processes with generic apparent size-dependent growth kinetics, and the results are exemplified for the model system of potassium dichromate in water. Potassium dichromate is a common inorganic chemical reagent. It is a crystalline ionic solid with a very bright, red-orange colour, with monoclinic crystals. It is mostly used as an oxidising agent in various laboratory and industrial application, however very limited information is available about the growth kinetics of the system. The ATR-UV/Vis probe was calibrated to provide real-time and *in situ* concentration measurement, which together with the CSD measurement was used

for model parameter identification (Aamir et al., 2009a). The results demonstrate that the novel seed recipe design approach, which considers practical constraints on the availability of seed CSDs resulting from sieve analysis in the model-based optimisation, can provide a desired target CSD, which is achievable in practice.

## 2. Experimental setup

### 2.1 Materials and Methods

In the experiments, potassium dichromate $(K_2Cr_2O_7)$ (>99.95% purity, Fisher BioReagents) solution was prepared, corresponding to a solubility of 20.0 g of anhydrous potassium dichromate per 100 g of water at 30 °C, using a 0.5 L jacketed crystallisation vessel equipped with thermocouple, ATR-UV/Vis spectrometer, focused beam reflectance measurement (FBRM) probes and a slurry recycle loop through a Malvern Mastersizer. Potassium dichromate was dissolved in water by heating to 40 °C at a rate of 0.8 °C/min. The solution was equilibrated at 40 °C for 20 min, to ensure complete dissolution of solids, which was also indicated by a decrease of the FBRM counts; then the temperature of the solution was reduced to 29 °C (one degree below saturation) at a rate of 0.5 °C/min. The temperature of the solution was maintained at 29 °C prior to the start of experiment, for 10 minutes, after which 1.2 g of sieved seed (in the size range between 106-125 μm) was added and the slurry was cooled to 20 °C over a duration of 60 minutes whilst following a cubic profile as shown in Figure 5 (a). During this period, the FBRM readings were monitored to check if any amount of the seed had dissolved or secondary nucleation occurred. The ATR-UV/Vis spectrometer was used to measure the absorbance throughout the experiment was and had previously been calibrated to provide *in situ* concentration measurements. A Malvern Mastersizer 2000 was used to measure on-line the CSD with a sampling time of 3 minutes.

### 2.2 Apparatus

The experimental setup is shown in Figure 1. The temperature in the 0.5 L jacketed glass vessel was controlled with a Pt100 thermocouple using a Huber VPC CC3 450 thermostat, controlled via a specially designed crystallisation control interface in Labview (National Instruments). An overhead stirrer with a four-bladed marine type impeller operated at 350 rpm was used to agitate the system. This agitation speed was chosen to be high enough to guarantee that particles were well suspended throughout the process, but low enough to avoid attrition or entrainment of bubbles due to vortex formation. An FBRM probe (model A100, Lasentec) was inserted into the solution to measure chord length distributions in the range of 0.8 to 1000 $\mu$m at intervals of 20 s. An ATR-UV/Vis spectrometer (model MCS 621, Carl Zeiss) with a deuterium source (UV-Vis/CLD 600) was used to measure the concentration. The absorbance was recorded every 20 s over a wavelength range of 240 – 720 nm, and

the absorbance values at a selected wavelength were used in a calibration to determine the concentration. The CSD was measured every three minutes using the Malvern Mastersizer 2000 laser-diffraction equipment. A peristaltic pump was used to circulate the slurry (solids with solvent) between the crystalliser and the Mastersizer. The length of the piping was minimised and the crystallisation experiments were carried out in a relatively narrow temperature range (29-20 °C) close to room temperature to avoid nucleation in the external loop. The initial solution at the initial temperature was circulated continuously throughout the tubes and Mastersizer, until a constant temperature was achieved in the whole system. After equilibration, the temperature was gradually decreased to 29 °C while maintaining the circulation of solution throughout the experimental setup to avoid nucleation in the silicon tubing. The FBRM probe was used to detect nucleation in the system. Samples were taken at the end of each batch for microscopic analyses. Images of the crystals produced were taken using a Leica DM LM microscope and a Leica PFC 350 FX camera.

## 2.3 Seed preparation

Seeds were prepared using a standard sieve analysis. The sieve sizes used were: 355 μm, 300 μm, 250 μm, 212μm, 180 μm, 150 μm, 125 μm, 106 μm, 90 μm, 75 μm, 60 μm and 40 μm, (coarser sieve sizes were placed on the top and finer at the bottom). The sieving time was set to 90 min, and the rotation and shaking caused the crystals to distribute throughout the sieve stack. The product obtained on the sieve size of 106 μm was collected for seeding in the parameter identification and validation experiments. The required amount of seed mass was achieved after running three batches of sieving, repeating the same procedure every time.

## 2.4 Concentration measurement using ATR-UV/Vis spectroscopy

The absorbance of the solution was measured using an ATR-UV/Vis spectrometer at different concentrations and temperatures. Figure 2 shows sample spectra of potassium dichromate solution in water at different concentrations. The spectrum of potassium dichromate system in water indicates two absorbance peaks at wavelengths 270.15 nm and 377.89 nm, respectively. For the calibration model the absorbance values were measured for several concentrations at different temperature ranges, as shown in Figure 3, covering both under-saturated and super-saturated conditions. A second order polynomial was fitted to the literature data (Mullin, 2001) to obtain the solubility curve, $C_{sat}(T) = 3.29 + 4.48 \cdot 10^{-1} T + 3.30 \cdot 10^{-3} T^2$, where $T$ is the temperature in $^{\circ}C$ and $C_{sat}$ is in g/g of water. A linear relationship among absorbance and concentration was observed for both wavelengths at 270.15 nm and 377.89 nm. Temperature has a small, linear effect on the absorbance and was taken into consideration in the calibration model, for which the following multi-linear form was adopted:

$$C = a_0 + a_1 A_1 + a_2 A_2 + a_3 T \,, \tag{1}$$

where $A_1$ and $A_2$ are the absorbance values at the two wavelengths 270.15 nm and 377.89 nm respectively, $C$ is the concentration (g/g solvent) and $T$ is the temperature (°C). The parameters for the calibration model ($a_i$ with $i = 0,1,...,3$) were estimated using the *fmincon* function in MATLAB, by a standard least-squares optimization approach. The optimisation problem for the parameter estimation is given by:

$$\min_{a_i} \sum_{k=1}^{K} (C_k - C_k^{\exp})^2 \,, \tag{2}$$

where $C_k$ and $C_k^{\exp}$ are the simulated and experimental concentration values at the discrete measurement conditions $k = 1,\ldots,K$, respectively, with $K$ being the number of measurement points. Various forms of the calibration model were evaluated and it was found that using the two peak absorbance values significantly improves the prediction accuracy of the calibration model. The parameters obtained with their uncertainty bounds (representing the 95% confidence intervals) are shown in Table 1. Figure 4 shows a comparison of estimated and simulated concentrations using the calibration model with parameters shown in Table 1, which are in good agreement, indicating that the simple form given by eq. (1) provides a very good calibration model. Hence a more complex robust chemometrics-based calibration was not considered necessary in this case. The validation point, which was not included in the calibration model development, also indicates the good accuracy of the calibration model (as shown in Figure 4). The excellent agreement between experimental and predicted concentrations and the very small error bounds on the parameters of the calibration model provide evidence that the ATR-UV/Vis with calibration models of relatively simple forms, can be used as a reliable *in situ* process analytical tool (PAT) for real-time concentration monitoring of crystallisation processes (Abu Bakar et al., 2009a) .

## 3. Population balance modelling of the Potassium Dichromate in water system using a combined QMOM-MOCH approach

Potassium dichromate is a fast growing system and no nucleation was observed during these experiments when a cubic temperature profile was followed. A cubic temperature profile is an experimental heuristic approximation of an optimal profile, which would generate a relatively constant supersaturation and maximize growth over nucleation for a given system (Mullin, 2001). Hence, considering a single growth direction, with one characteristic length $L$, and a well-mixed crystallizer with growth as the only dominating phenomena the population balance equation (PBE) has the form:

$$\frac{\partial f_n(L,t)}{\partial t} + \frac{\partial (G(S,L;\theta_g) f_n(L,t))}{\partial L} = 0\,, \tag{3}$$

where $f_n(L,t)$ is the crystal size distribution expressed as a number density function (number of crystals per unit mass of solvent and size), $t$ is time, $G(S,L;\theta_g)$ is the rate of crystal growth, $S = (C - C_{sat})$ is the absolute supersaturation, $C$ is the solute concentration (g/g solvent), $C_{sat} = C_{sat}(T)$ is the saturation concentration with $T$ being the temperature, and $\theta_g$ is a vector of growth parameters. The solution of eq. (3) is an initial value problem, with initial condition given by the size distribution of the seeds, $f_n(L,0) = f_{n,0}(L_0)$. The generic PBE in eq. (3) can be reduced to a system of ODEs by applying the method of characteristics (MOCH). The aim of the MOCH is to solve the PBE by finding characteristic curves in the $L-t$ plane that reduce the partial differential equation to a system of ODEs (Aamir et al., 2009b, Hounslow and Reynolds, 2006). In the case of generic growth kinetics, eq. (3) can be rewritten in the form of,

$$\frac{\partial f_n(L,t)}{\partial t} + G(S,L;\theta_g)\frac{\partial f_n(L,t)}{\partial L} = -f_n(L,t)\frac{dG(S,L;\theta_g)}{dL}\,, \tag{4}$$

and the characteristic equations are given by the following system of ODEs:

$$\frac{dL}{dt} = G(S,L;\theta_g)\,, \tag{5}$$

$$\frac{df_n(L,t)}{dt} = -f_n(L,t)\frac{dG(S,L;\theta_g)}{dL}\,, \tag{6}$$

with initial conditions $L = L_0$ and $f_n(L,0) = f_{n,0}(L_0)$, i.e. the seed CSD. To obtain the dynamic evolution of the crystal size distribution $f_n(L,t)$, eqs. (5) - (6), with a given growth rate expression, can be integrated repeatedly for different initial values $[L_0, f_{n,0}(L_0)]$ (Aamir et al., 2009b). The growth rate is generally a function of the supersaturation, $S$, which can be calculated from the material balance. The solute concentration is given by,

$$C(t) = C(0) - k_v \rho_c (\mu_3(t) - \mu_3(0))\,, \tag{7}$$

where $\rho_c$ is the density of crystals, $k_v$ the volumetric shape factor, $C(0)$ is the initial concentration, $\mu_3(0)$ is the initial third moment (of the seed), whereas $C(t)$ and $\mu_3(t)$ are the concentration and third moment of the CSD at any time $t$, respectively. The solution of eqs. (5) -(6) and (7) requires *a priori*

knowledge of the dynamic evolution of the supersaturation, $S(t)$ and/or the third moment $\mu_3(t)$, which can be obtained by using the moment transformation of eq. (3) via the standard method of moments (in the case of size-independent growth and nucleation) or QMOM (in more generic cases including apparent size-dependent growth, breakage and aggregation). Both methods calculate the evolution of the moments of the distribution. Alternatively the moments could be calculated from the discretized size distribution resulting from the MOCH, simultaneously with the integration of the ODEs (5) and (6). In the case of the potassium dichromate system in water apparent size-dependent growth kinetics was observed, which can be described by

$$G = k_g S^g (1+\gamma L)^p, \tag{8}$$

where $\theta_g = [k_g, g, \gamma, p]$ is the growth parameter vector. Hence applying the moment transformation to eq. (3) using the quadrature approximation of the resulting moment equations in the case of size-dependent growth the following set of ordinary differential equations results (Marchisio et al., 2003a; Marchisio et al., 2003b; McGraw, 1997),

$$\begin{aligned} &\frac{d\mu_0}{dt} = 0, \\ &\frac{d\mu_j}{dt} = j\sum_{i=1}^{N_q} \alpha_i L_i^{j-1} G\left(S, L_i; \theta_g\right), \quad j = 1,2,3,...,\infty \end{aligned} \tag{9}$$

where the $j$th moment $\mu_j$ and its quadrature approximation are defined by

$$\mu_j = \int_0^{+\infty} f_n(L) L^j dL \approx \sum_{i=1}^{N_q} \alpha_i L_i^j, \quad j = 0,1,\ldots,\infty. \tag{10}$$

In eq. (10) $N_q$ is the number of quadrature points, $\alpha_i$ and $L_i$, $i = 1,\ldots,N_q$ are the weights and abscissas, respectively, in the quadrature approximations, which can be calculated e.g. by using a product difference algorithm (McGraw, 1997) or via direct solution of a differential-algebraic equation system that results by setting the condition of no error if the integral from the moment definition is replaced with its quadrature approximation (Gimbun et al., 2009) . Note that the abscissas $L_i$, in the QMOM part of the algorithm are used to compute the moments only and are different from the characteristic length $L$ used to characterize the particle size in the PBE and in the MOCH part of the algorithm.

## 4. Model Identification and Validation

The size-dependent growth parameters were determined for the batch cooling crystallisation of the inorganic compound, potassium dichromate ( $K_2Cr_2O_7$ ) in water. The experimental data were obtained using a laboratory scale crystallisation system. The operating conditions for the identification and validation experiments are shown in Table 2. In experiment A, a cubic profile (Figure 5 (a)) was followed throughout the batch, whereas in experiment B simple linear cooling (Figure 5 (b)) was used. Seed was introduced in both cases shortly after the supersaturated state had been reached.

Figure 5 (a) indicates that in the case of experiment A, (with cubic cooling profile) no nucleation happened during the crystallisation since the FBRM number of counts/s is practically constant throughout the batch after the initial increase at $t = 0$, corresponding to the seed addition. However in experiment B some secondary nucleation was observed, as shown in Figure 5 (b). This secondary nucleation is observed around 35 minutes from the start of the batch and is the result of the too fast supersaturation generation by the linear cooling profile. Experiment A was used for model parameter identification with the PBM solved using the QMOM-MOCH approach described in Section 3, whereas experiment B was used for validation purposes. The generic apparent size-dependent growth expression, given by eq. (8), was used in the model identification. The optimization problem for the parameter estimation is given by,

$$\min_{\theta} \left\{ w_f \sum_{k=1}^{K} \sum_{l=1}^{N_d} (f_{v,k}(L_l) - f_{v,k}^{\exp}(L_l))^2 + w_C \sum_{k=1}^{K} (C_k - C_k^{\exp})^2 \right\}, \tag{11}$$

$$\text{subject to} \qquad \theta_{\min} \le \theta \le \theta_{\max}, \tag{12}$$

with $\theta = [k_g, g, \gamma, p]$ being the model parameter vector with the growth kinetic parameters, $\theta_{\min}$ and $\theta_{\max}$ are vectors with specified minimum and maximum bounds for each parameter, respectively, $C_k$ and $C_k^{\exp}$ are the simulated and experimental concentration values at the discrete time steps $k = 1,\ldots,K$, $f_{v,k}$ and $f_{v,k}^{\exp}$ are the values of the simulated and experimental volume particle density functions, corresponding to the discretized size $L_l$, $l = 1,\ldots,N_d$, with $N_d$ being the number of experimental size bins, and $w_f$, $w_C$ are objective function weighting factors. The simulated volume pdf is computed from the number pdf as:

$$f_{v,i} = f_{n,i} L_i^3 \,/\, \sum_{i=1}^{N_d} (f_{n,i} L_i^3 \Delta L_i). \tag{13}$$

The optimization problem is solved using a sequential quadratic programming (SQP) based optimization approach implemented in the Matlab function *fmincon*. The resulting model parameters

with the 95% confidence intervals, for the potassium dichromate system are presented in Table 3. The confidence intervals were obtained using the method described in detail in Nagy et al., 2008. The dynamic evolution of the modelled and experimental CSDs are in very good agreement during the entire batch, as shown in Figure 6. It can be seen that due to the particular size-dependent growth kinetics of this system, the CSD broadens with decreasing height during the batch. The PBM with the identified growth parameters is able to describe the main features of the CSD throughout the entire batch, confirming that an apparent size-dependent growth mechanism is suitable to consider for this system.

Figure 7(a) and (b) show the comparison between the experimental and model predicted concentration and weight mean size ($d_{43}$) throughout the batch, which are also in very good agreement. The weight mean size is is calculated as the ratio between the forth third moments of the CSD, $d_{43} = \mu_4 / \mu_3$.

The linear profile was used for model validation and Figure 8 shows a comparison of the experimental data and model predictions for the CSD and concentration from experiment B. Figure 8(a) indicates that towards the end of the batch the CSD is slightly over predicted, which corresponds to higher consumption of solute concentration in the simulation, as shown in Figure 8(b). Additionally, Figure 8(a) indicates the appearance of a small (as volume pdf) secondary peak in the experimental CSD at around 35 min during the process, which is due to the secondary nucleation event detected by the FBRM approximately at the same time (see Figure 5(b)). This nucleation event is not considered in the model, which is based only on the growth kinetics, and hence also contributes to the over-prediction of the measured CSD by the simulation. Nevertheless, the maximum difference between the simulated and the experimental concentration is only 6.5%. For both experiments (A and B) the same masses and sizes of seed were used (the seed was retained between sieve sizes 106-125 μm, as described in Table 2). A sample microscopic image of the seed used in the experiments is shown in Figure 9(a). Microscopic images of the products obtained at the end of experiments A, shown in Figure 9(b), and for B, shown in Figure 9(c), indicate that the crystals obtained at the end of the cubic profile are larger and more uniform in size with few fines and very few agglomerates. However, the crystals obtained at the end of the linear profile are smaller, more agglomerated, and with clear evidence of the existence of finer particles due to secondary nucleation, also indicated by the CSD measurement shown in Figure 8(a).

## 5. Seed recipe optimisation for designing the shape of the product CSD

Seed recipes can be optimised to obtain a desired target CSD. Experimentally, seed can be obtained by mixing different amounts of seeds with different size distributions (Aamir et al., 2009a; Doki et al., 2001; Kalbasenka et al., 2007; Kubota et al., 2001). According to the proposed method here, the seed recipe is represented by a sum of Gaussian distributions, with each Gaussian corresponding to the

seed distribution in a particular sieve size range, and the generic optimisation problem with the objective of shaping the distribution at the end of batch is formulated as follows:

$$\min_{m_{seed},w_i|_{i=1,\ldots,N_G}} \sum_{i=1}^{N_d} (f_{v,i}(t_{batch}) - f_{v,i}^{tar})^2 , \tag{14}$$

$$\text{subject to:} \quad \sum_{i=1}^{N_G} w_i = 1 , \tag{15}$$

$$0 \le w_i \le 1 \quad \text{for } i = 1,\ldots,N_G , \tag{16}$$

$$0 < m_{seed} < 0.1C(0)m_{sol} , \tag{17}$$

$$C(t_{batch}) \le C_{f,\max} , \tag{18}$$

$$f_{n,seed}(L) = \frac{m_{seed}}{m_{sol}} \frac{1}{\rho_c k_v} \sum_{i=1}^{N_G} \frac{w_i}{L_{m,i}^3} \mathcal{N}_i(L; L_{m,i}, \sigma_i), \text{ with } \mathcal{N}_i(L; L_{m,i}, \sigma_i) = \frac{1}{\sqrt{2\pi}\sigma_i} e^{-(L-L_{m,i})^2/(2\sigma_i^2)} \tag{19}$$

where $m_{seed}$ is the total seed mass (g), $w_i$ are the weight fractions of seeds from a particular sieve fraction in the final seed mixture, $i = 1,2,\ldots,N_G$, $N_G$ is the number of Gaussians corresponding to the CSDs of a particular seed fraction, $L_{m,i}$ the mean sizes (μm), $\sigma_i$ (μm) the standard deviations of the respective Gaussian distributions, $m_{sol}$ is the mass of water used as solvent (g), $C(0)$ and $C(t_{batch})$ are the solute concentrations at the beginning and end of the batch, respectively. The constraints given by inequalities (17) restrict the amount of seed added to a maximum of 10% of the mass of solid dissolved in the system whereas the constraint given by (18) is a productivity constraint with $C_{f,\max}$ being the maximum acceptable concentration at the end of the batch to achieve the required yield. The objective function is expressed as the sum square error between the simulated ($f_{v,i}$), and target ($f_{v,i}^{tar}$) volume pdfs, respectively.

The seed recipe design method given by eqs. (14)-(19) is formulated for the practical situation when the mean and standard deviations characterizing the seeds in a particular size ranges are fixed, being determined by the method and equipment (e.g. milling, sieving) used to produce the particles, and only the total amount of seed and the weight fractions in which the various size ranges are mixed together are optimised, with the vector of decision variables being defined as $[m_{seed}, w_1, w_2, \ldots, w_{N_G}]$. One of the most common methods to generate seed is sieving using standard sieve sizes. Hence, the seed recipe was optimised for fixed mean and standard deviations based on the selection of relevant sieves. Generally these values are material dependent and would be given for a particular system. Note that although eq. (19) expresses the seed recipe as a sum of Gaussian distributions, it is possible to formulate the seed recipe in terms of a sum of any distribution or combination of distributions, and

eventually these distributions should be represented by the actual experimental CSDs resulting from the analysis of each seed fraction. Hence this formulation would allow designing seed recipes in which various seed fractions could be produced differently (e.g. mixtures of seeds from various milling equipment and/or crystalline seed, etc.), and their distribution could be given by different types of distribution functions. In this work, for generality, the mean values of the seed distributions were calculated as the arithmetic means of the consecutive sieve sizes and the standard deviations were considered to be equal to half of the size ranges determined by the corresponding sieves,

$$L_{m,i} = (\mathcal{L}_i + \mathcal{L}_{i+1}) / 2 , \tag{20}$$

$$\sigma_i = (\mathcal{L}_{i+1} - \mathcal{L}_i) / 2 , \tag{21}$$

where $\mathcal{L}_i$, $i = 0,1,...,N_G$, are the standard sieve sizes, with $N_G$ being equal to the total number of selected sieves used in the optimisation. These values provide approximately a $2\sigma$ overlap between the distributions of seeds from adjacent sieve ranges, and correspond to the experimental observations of the sieve analyses of the studied compound. The seed can be designed for any target CSD, e.g. bimodal or tri-modal distributions. The target bimodal and tri-model distributions used for the simulations are expressed as:

$$f^{tar}_{n,\text{bimodal}} = 0.25\frac{1}{\sqrt{2\pi}2.44}e^{-(L-320)^2/(2.44^2)} + 0.75\frac{1}{\sqrt{2\pi}2.74}e^{-(L-650)^2/(2.74^2)} , \tag{22}$$

$$f^{tar}_{n,\text{tri-modal}} = 0.75\frac{1}{\sqrt{2\pi}2.20}e^{-(L-250)^2/(2.20^2)} + 0.22\frac{1}{\sqrt{2\pi}2.62}e^{-(L-450)^2/(2.62^2)} + 0.03\frac{1}{\sqrt{2\pi}2.38}e^{-(L-660)^2/(2.38^2)}, \tag{23}$$

where equations (22) and (23) generate the target number density functions, which were converted to a volume pdf using the equation (13) and were used in the optimisation. Figure 10 shows the result of the seed design, for the two arbitrary target distributions. For these simulations it was assumed that the supersaturation was constant throughout the batch at a value of $S = 0.0005$ g/g water. The batch time used in the optimisations was 60 minutes and the initial concentration used was 0.2 g/g water. The details of the optimised seeds for the two target distributions are shown in Table 4. Seven consecutive seed fractions represented by the set $\mathcal{L} = \{37-74, 74-105, 105-177, 177-210, 210-250, 250-297, 297-354\}$, with sieve sizes in μm, were used to optimise the seed distribution for the bimodal (target) distribution. Figure 10(a) indicates that the resulting CSD is in good agreement with the desired bimodal CSD. The optimisation automatically selected the optimal set of sieves consisting of the first five sieve sizes, $\mathcal{L}^* = \{37-74, 74-105, 105-177, 177-210, 210-250\}$ and hence the optimal seed distribution is a sum of five Gaussian distributions ($N^*_G = 5$). The amounts for the other sieve ranges were automatically set to zero by the optimizer indicating that those sieve fractions are not needed for the

seed recipe. The mean values, standard deviations and weight fractions for these consecutive sieve sizes are shown in Table 4. If a more complex, tri-modal target CSD is used, as shown in Figure 10(b) and the optimization is solved with a slightly different set of six sieve fractions (sieve sizes in μm), $\mathcal{L} = \{37-44,\, 44-74,\, 74-200,\, 200-250,\, 250-297,\, 297-354\}$ the optimal seed distribution consists of a sum of only three Gaussians and the set of selected sieve ranges were $\mathcal{L}^* = \{44-74,\, 74-200,\, 200-250\}$. The means, standard deviations and weight fractions for these consecutive sieve sizes are also shown in Table 4. The results indicate that the optimal seed recipe strongly depends on the available sieve fractions, and an apparently more complex target distribution may be achieved with smaller number of seed fractions. However, in the case of growth only processes the number of seed size fractions will be at least equal to the number of modes in the target distribution. The target and the simulated distributions are in good agreement. The optimised seed masses for the bimodal and tri-modal distribution were 0.95 g and 1.93 g, respectively. For the simulation purpose the required yield was 33%, and was achieved in both cases.

## 6. Experimental evaluation of CSD design using mixture of seeds

To evaluate the seed design methodology for mixture of different seeds an arbitrary bimodal number distribution was selected as a target:

$$f_n^{tar} = 0.72\frac{1}{\sqrt{2\pi}2.40}e^{-(L-280)^2/(2.40^2)} + 0.28\frac{1}{\sqrt{2\pi}2.68}e^{-(L-470)^2/(2.68^2)}\ . \tag{24}$$

Equation (24) was converted to a volume pdf using eq. (13) and was taken as the target distribution in an optimisation problem defined similarly to eqs (14)-(19). The target distribution is shown in Figure 11 (b). In the seed recipe optimisation consecutive sieve sizes were used, which defined a set of seven sieve size ranges $\mathcal{L} = \{37-88,\, 88-105,\, 105-177,\, 177-210,\, 210-250,\, 250-297,\, 297-354\}$. The optimal seed is the result of a mixture of four Gaussian distributions with parameters, $w = [0.73,\, 0.02,\, 0.23,\, 0.02]$, $L_m = [62.5\,\mu\text{m},\, 96.5\,\mu\text{m},\, 141.0\,\mu\text{m},\, 193.5\,\mu\text{m}]$ and $\sigma = [25.5\,\mu\text{m},\, 8.5\,\mu\text{m},\, 36\,\mu\text{m},\, 16.5\,\mu\text{m}]$ corresponding to the selected sieve size ranges of $\mathcal{L}^* = \{37-88,\, 88-105,\, 105-177,\, 177-210\}$ and the optimised mass of seed was $1.214$ g. The optimised seed distributions and masses were calculated for the cubic temperature profile of experiment A (as shown in Figure 5 (a)).

An experiment was designed to achieve the target bimodal distribution described by eq. (24). The sieve analysis of the raw material indicated that the seed fractions available in considerable quantity were only in the size ranges of 40-63, 63-90 and 90-106 μm. Hence the seed recipe optimisation was

performed again for these size ranges only. The optimised seed was a mixture of two Gaussians with parameters $w = [0.50, 0.50]$, $L_m = [51.5\,\mu\text{m}, 98\,\mu\text{m}]$ and $\sigma = [11.5\,\mu\text{m}, 8\,\mu\text{m}]$ corresponding to the selected sieve sizes of 40-63 and 90-106 µm and the optimised mass of seed was 1.118 g. Hence, the seed used for the experiment was a blend of two sieve fractions retained between 40-63 µm and 90-106 µm. Figure 11(a) shows the comparison between the optimised seed as four Gaussians, the optimal seed as two Gaussians, and the actual seed used for the experiment (measured using the Malvern Mastersizer). It can be observed that the experimental and optimal seed distributions are very close, although the two optimal seeds were blends of different sieve size ranges in different amounts (weight fractions). These results indicate that a particular optimal seed CSD can be the result of blending different sieved seed fractions. The optimal seed recipe resulting from the mixture of the two seed fractions was used in an experiment with a cubic temperature trajectory (the same as used in experiment A), cooling the solution from 29 °C to 20 °C during a 60 minutes duration using the experimental setup as described in section 2. The initial concentration of the system was 0.20 g/g water corresponding to an equilibrium temperature of 30 °C and seed was added at 29 °C.

Figure 11(b) shows a comparison between the target and the experimental CSDs at the end of the batch. The final product CSD measured is shifted towards slightly smaller particles compared to the target distribution. Nonetheless, the seed recipe design procedure was able to provide a product distribution which is remarkably close to the target distribution. The difference between the target and product CSDs may be caused by the discrepancy between the theoretical optimal seed recipe and the actual seed recipe prepared experimentally as shown in Figure 11(a). Although the differences in the seed CSDs are small, they may be amplified during the crystallisation processes, leading to increasingly larger errors between the experimental and target CSD. Additionally, although the model identification indicated that the process model is in very good agreement with the experimental data a certain level of model prediction error is present, which may lead to errors in the theoretical seed recipe. To further evaluate this, a simulation was carried out using the measured experimental seed CSD as initial condition in the model. Figure 11 (b) shows that the experimental and simulated CSDs are very close when the model was initiated with the measured experimental seed. These results indicate that the model prediction is very good, and the difference between the target and experimental product CSDs is caused by the accumulating prediction error due to the discrepancy between the optimal and experimental seed recipes.

The absorbance was measured using the ATR-UV/Vis spectrometer throughout the experiment and was converted to concentrations, using the parameters shown in Table 1. A comparison between the simulated and experimental concentrations is shown in Figure 12. The simulated concentration falls below the experimental concentration (error of 1.74%), which also agrees with the discrepancy between the experimental and target CSDs. However when the simulations are initiated with the

experimental seed CSD, the simulated and experimental concentration profiles are in very good agreement, reinforcing that model developed with the identified kinetic parameters, describes very well the real process. Figure 13 (a and b) show the microscopic images for the mixture of the seed and the final distribution obtained at the end of the experiment and indicate that the final distribution of crystals is indeed a mixture of two different sizes.

To provide further experimental evidence of the seed recipe design approach an additional target bimodal distribution was designed, given by

$$f_n^{tar} = 0.60 \frac{1}{\sqrt{2\pi}2.18} e^{-(L-210)^2/(2.18^2)} + 0.40 \frac{1}{\sqrt{2\pi}2.76} e^{-(L-370)^2/(2.76^2)} \quad (25)$$

To carry out the experiments, the seed was optimised using the available sieve sizes, 40-63 μm and 90-125 μm. The optimised seed was a mixture of two Gaussians with weight fractions $w = [0.54, 0.46]$. The means and standard deviations of the seed fractions are $L_m = [51.5\,\mu\text{m}, 107.5\,\mu\text{m}]$ and $\sigma = [11.5\,\mu\text{m}, 17.5\,\mu\text{m}]$, respectively, corresponding to the sieve sizes of 40-63 and 90-125 μm. The optimised mass of seed was 1.115 g. Figure 14 (a) shows the comparison between the optimised seed as two Gaussians and the actual seed used for the experiment (measured using Malvern Mastersizer). It can be observed that the experimental and optimal seed distributions are close but not in as good agreement as in the previous case. For the second seed blend the experiment was carried out under the same conditions as for the first seed blend. The same cubic temperature trajectory was used as given for experiment A, cooling the solution from 29°C to 20°C during a 60 minutes period. The initial concentration of the system was 0.20 g/g water corresponding to an equilibrium temperature of 30°C and seed was added at 29°C. The experimental characteristics of the optimised seed recipes for both experiments are summarised in Table 5.

Figure 14 (b) shows the comparison between the target and the experimental CSDs resulting at the end of the batch for the second arbitrary bimodal distribution. The final product CSD showed smaller but broader peaks than the target distribution. Overall the shape of the product distribution is close to the target distribution, relative to the differences in the experimental and optimal seeds, indicating that the seed recipe design procedure was able to provide a product CSD relatively close to a desired target. The comparison between the simulated and experimental concentrations is shown in Figure 14 (c). The simulated concentration indicates a higher solute consumption, which is also in correlation with the discrepancy between the experimental and target distributions. The difference between measured and simulated concentrations at the end of the batch is 4.63%. This is greater than in the previous experiment (1.73%), which is also in correlation with the larger difference between the target and experimental CSDs, and is the result of the more significant discrepancy between the optimal and experimental seed CSDs, compared to the experiments with seed blend 1. Figure 15 (a and b) show

the microscopic images for the mixture of the seed and the final distribution obtained at the end of the experiment for the second seed blend. The microscopic images also indicate that the both the seed and the final distribution of crystals are mixtures of two different size ranges. The experimental results indicate that it is possible to achieve a desired multimodal distribution by a model-based optimal design of an appropriate seed blend from various fractions of sieved seeds. The methodology provides a systematic approach to obtain seed mixture recipes by using available sieve sizes, which will yield the required shape of the product CSD, to achieve e.g. a desired therapeutic effect by designing dissolution profiles, or to achieve improved packing properties during the formulation of the final product.

## 7. Conclusions

The paper describes an approach for optimal seed recipe design for crystallisation processes, by automatically determining, using a population balance model-based optimisation, the amounts of seeds from various sieved seed fractions required to achieve a desired shape of the product CSD. To evaluate the methodology an experiment was carried out for the potassium dichromate–water system. Kinetic parameters of the apparent size-dependent growth rate expression were identified using an experimental setup with and *in situ* ATR-UV/Vis probe and on-line Mastersizer for real-time concentration and crystal size distribution measurements, respectively. The parameters were used to optimise the seed recipe by mixing different amounts of sieved seed fractions. Seed mixtures were represented as a sum of Gaussian distributions, with each Gaussian corresponding to the seed distribution in a particular sieve size range. Experimental results were in good agreement with the model-based CSD design, providing evidence that it is possible to achieve a desired multimodal product distribution by designing appropriate seed mixtures from various fractions of sieved seeds. The paper also illustrates the simultaneous application of *in situ* process analytical tools, such as focused beam reflectance measurement (FBRM) for nucleation detection, attenuated total reflection (ATR) UV/Vis spectroscopy for concentration monitoring, as well as the in-line use of a Mastersizer for real-time CSD measurement in the case of the potassium dichromate in water system.

## Acknowledgements

Financial support provided by the Engineering and Physical Sciences Research Council (EPSRC), U.K., (grant EP/E022294/1) is gratefully acknowledged.

## References

Aamir, E., Nagy, Z.K., Rielly, C.D., 2009a. Seed recipe design for shaping the crystal size distribution for supersaturation controlled crystallisation processes., 16th Int. Workshop on Industrial Crystallisation, Lappeenranta, Finland.

Aamir, E., Nagy, Z.K., Rielly , C.D., Kleinert, T., Judat, B., 2009b. Combined quadrature method of moments and method of characteristics approach for efficient solution of population balance models for dynamic modeling and crystal size distribution control of crystallisation processes. Ind. Eng. Chem. Res. 48, 8575-8584.

Abbott, N.L., 2001. New horizons for surfactant science in chemical engineering. AIChE J. 47, 2634-2639.

Abu Bakar, M.R., Nagy, Z.K., Rielly, C.D., 2009a. Seeded batch cooling crystallisation with temperature cycling for the control of size uniformity and polymorphic purity of sulfathiazole crystals. Org. Process Res. Dev. 13, 1343-1356.

Abu Bakar, M.R., Nagy, Z.K., Saleemi, A.N., Rielly, C.D., 2009b. The impact of direct nucleation control on crystal size distribution in pharmaceutical crystallisation processes. Cryst. Growth Des. 9, 1378-1384.

Adi, H., Larson, I., Stewart, P., 2007. Use of milling and wet sieving to produce narrow particle size distributions of lactose monohyrate in the sub-sieve range. Powder Technol. 179, 95-99.

Bohlin, M., Rasmuson, A.C., 1996. Application of controlled cooling and seeding in Batch Crystallisation. Can. J. Chem. Eng. 70, 120-126.

Braatz, R.D., 2002. Advanced control of crystallisation processes. AIChE J. 26, 87-99.

Chung, S.H., Ma, D.L., Braatz, R.D., 1999. Optimal seeding in batch crystallisation. Can. J. Chem. Eng. 77, 590-595.

Chung, S.H., Ma, D.L., Braatz, R.D., 2000. Optimal model-based experimental design in batch crystallisation. Chemom. Intell. Lab. Syst. 50, 83-90.

Doki, N., Kubota, N., Sato, A., Yokota, M., 2001. Effect of cooling mode on product crystal size in seeded batch crystallisation of potassium alum. Chem. Eng. J. 81.

Doki, N., Seki, H., Takano, K., Asatani, H., Yokota, M., Kubota, N., 2004. Process control of seeded batch cooling crystallisation of the metastable alpha-form glycine using an in-situ ATR-FTIR spectrometer and an in-situ FBRM particle counter. Cryst. Growth Des. 4, 949-953.

Fujiwara, M., Nagy, Z.K., Chew, J.W., Braatz, R.D., 2005. First-principles and direct design approaches for the control of pharmaceutical crystallisation. J. Process Control 15, 493-504.

Gimbun, J., Nagy, Z.K., Rielly, C.D., 2009. Simultaneous quadrature method of moments for the solution of population balance equations, using a differential algebraic equation framework. Ind. Eng. Chem. Res. 48, 7798-7812.

Grosso, M., Galan, O., Barratti, R., Romagnoli, J. A., 2009. A novel approach for the prediction of PSD in anti-solvent mediated crystallisation. Chem. Eng. Sci. 27, 291-296.

Heffels, C.M.G., Kind, M., 1999. Seeding technology: an underestimated critical success factor for crystallisation., 14th International Symposium on Industrial Crystallisation., pp. 2234-2246.

Hounslow, M.J., Reynolds, G.K., 2006. Product engineering for crystal size distribution. AIChE J. 52, 2507-2517.

Jagadesh, D., Kubota, N., Yokota, M., Doki, N., 1999. Seeded effect on Batch Crystallisation of Potassium Sulfate under Natural Cooling mode and a simple Design Method of Crystallizer. J. Chem. Eng. Jpn. 32, 514-520.

Kalbasenka, A.N., Spierings, L.C.P., Huesman, A.E.M., Kramer, H.J.M., 2007. Application of seeding as a process actuator in a model predictive control framework for fed-batch crystallisation of ammonium sulphate. Part. Part. Syst. Charact. 24, 40-48.

Kubota, N., Doki, N., Yokota, M., Sato, A., 2001. Seeding policy in batch cooling crystallisation. Powder Technol. 121, 31-38.

Larsen, P.A., Patience, D.B., Rawlings, J.B., 2006. Industrial crystallisation process control. IEEE Control Systems Magazine 26, 70-80.

Liotta, V., Sabesan, V., 2004. Monitoring and feedback control of supersaturation using ATR-FTIR to producean active pharmaceutical ingredient of a desired crystal size. Org. Process Res. Dev. 8, 488-494.

Ludwick, J.C., Henderso, P.L., 1968. Particle shape and inference of size from sieving. Sedimentology 11, 197-235.

Lung-Somarriba, B.L.M., Moscosa-Santillan, M., Porte, C., Delacroix, A., 2004. Effect of seeded surface area on crystal size distribution in glycine batch cooling crystallisation: a seeding methodology. J Cryst. Growth 270, 624-632.

Mangin, D., Garcia, E., Gerard, S., Hoff, C., Klein, J.P., Veesler, S., 2006. Modeling and dissolution of a pharmceutical compound. J. Cryst. Growth 286, 121-125.

Marchisio, D.L., Pikturna, J.T., Fox, R.O., Vigil, R.D., Barresi, A., 2003a. Quadrature method of moments for population-balance equations. AlChE J. 49, 1266-1276.

Marchisio, D.L., Vigil, R.D., Fox, R.O., 2003b. Quadrature method of moments for aggregation–breakage processes. J. Colloid Interface Sci. 258.

McGraw, R., 1997. Description of aerosol dynamics by the quadrature method of moments. Aerosol Sci. Technol. 27, 255-265.

Middlebrooks, S.A., 2001. Modelling and control of Silicon and Germanium thin film chemical vapor deposition. University of Wisconsin-Madison.

Mullin, J.W., 2001. Crystallisation, Fourth ed. Butterworth Heinemann, Oxford, UK.

Nagy, Z.K., Braatz, R.D., 2003. Robust nonlinear model predictive control of batch processes. AIChE J. 49, 1776-1786.

Nagy, Z.K., Chew, J.W., Braatz, R.D., 2008. Comparative performance of concentration and temperature controlled crystallisation. J. Process Control 18, 399-407.

Nagy, Z.K., Fujiwara, M., Woo, X. Y., Braatz, R.D., 2008. Determination of the kinetic parameters for the crystallisation of paracetamol from water using metastable zone width experiments. Ind. Eng. Chem. Res. 47, 1245-1252.

Olesberg, J.T., Arnold, M.A., Hu, S.-Y.B., Wiencek, J.M., 2000. Temperature-Insensitive Near-Infrared Method for Determination of Protein Concentration during Protein Crystal Growth. Analytical Chemistry 72, 4985-4990.

Rawlings, J.B., Miller, A.G., Witkowaski, W.R., 1993. Model identification and control of solution crystallisation processes: A review. Ind. Eng. Chem. Res. 32, 1275-1296.

Ruf, A., Worlitschek, J., Mazzotti, M., 2000. Modeling and experimental analysis of PSD measurements through FBRM. Part. Part. Syst. Charact. 17, 167-179.

Shi, D., Mhaskar, P., El-Farra, N.H., Christofides, P.D., 2005. Predictive control of crystal size distribution in protein crystallisation. Nanotechnology 16, S562-S574.

Simon, L.L., Elias,Y., Nagy, Z.K., Hungerbuhler, K., 2009a. Impact of seed particle size distribution uncertainty on the supersaturation controlled batch cooling crystallisation time: experimental and model Based Evaluation. AIChE meeting, Nashville USA.

Simon, L.L., Nagy, Z.K., Hungerbuhler, K., 2009b. Comparison of external bulk video imaging with focused beam reflectance and ultra violet-visible spectroscopy for metastable zone identification in food and pharmaceutical crystallisation processes. Chem. Eng. Sci., 64, 3344-3351

Simon, L.L., Nagy, Z.K., Hungerbuhler, K., 2009c. Endoscopy-based in situ bulk video imaging of batch crystallisation processes. Org. Process Res. Dev., 13 (6), 1254-1261)

Ward, J.D., Mellichamp, D.A., Doherty, M.F., 2006. Choosing an operating policy for seeded batch crystallisation. AIChE J. 52, 2046-2054.

Wibowo, C., Chang, W.-C., Ng, K.M., 2001. Design of integrated crystallisation systems. AlChE J. 47, 2474-2492.

Wibowo, C., Ng, K.M., 2001. Operational Issues in Solids Processing Plants: Systems View. AIChE J. 47, 107-125.

Wiencek, J.M., 2002. Crystallisation of proteins, in: Myerson, A.S. (Ed.), Handbook of industrial crystallisation, 2nd ed. Butterworth-Heinemann, pp. 267-285.

Woo, X.Y., Nagy, Z.K., Tan, R.B.H., Braatz, R.D., 2009. Adaptive concentration control of cooling and antisolvent crystallisation with laser backscattering measurement. Cryst. Growth Des. 9, 182-190

Worlitschek, J., Mazzotti, M., 2004. Model based optimization of particle size distribution in batch cooling crystallisation of Paracetamol. Cryst. Growth Des. 4, 891-903.

Xie, W., Rohani, S., Phoenix, A., 2001. Dynamic modelling and operation of a seeded batch cooling crystalliser. Chem. Eng. Commun. 187, 229-249.

Yannick E., Nagy Z.K., Hungerbuhler K, 2009. Evaluation of sieving for seed production and crystallisation recipe design. 8th World Congress of Chemical Engineering (WCCE8), Montreal, Canada.

Yu, Z.Q., Chow, P.S., Reginald, B.H.T., 2006. Seeding and constant-supersaturation control by ATR-FTIR in anti-solvent crystallisation. Org. Process Res. Dev. 10, 717-722.

Zhang, G.P., Rohani, S., 2003. On-line optimal control of a seeded batch cooling crystallizer. Chem. Eng. Sci. 58, 1887-1896.

# List of Figures

Figure 1: A schematic representation of the experimental setup.

Figure 2: UV/Vis spectra of potassium dichromate in water at different concentrations obtained using in situ ATR-UV/Vis spectroscopy.

Figure 3: Measurement points for absorbance values for the used concentrations and temperature ranges including solubility curve (Mullin, 2001) and the observed nucleation points.

Figure 4: Estimation and validation of calibration parameters using measured and simulated concentration.

Figure 5: Total counts measured by FBRM throughout the entire batch a) when the cubic profile b) when the linear profile was run for duration of 60 minutes.

Figure 6: Dynamic evolution of the modelled and experimental CSD for Potassium dichromate $H_20$ system for experiment A.

Figure 7: Experimental and simulated results: a) concentration b) De Broucker mean diameter during the entire batch of experiment A.

Figure 8: Experimental and simulated results for experiment B to validate the modal parameters. a) Dynamic evolution of CSD b) concentration during the entire batch of experiment B.

Figure 9: Microscopic image of the a) seed distribution and b) crystals obtained at the end of experiment A (cubic profile) c) crystals obtained at the end of experiment B (linear profile).

Figure 10: a) Optimised seed for a bimodal target CSD; (b) optimised seed for tri-modal target CSD.

Figure 11: **a) Comparison of experimental and optimal seed distribution. b) Comparison of experimental and target distribution (for which a mixture of seed was optimised) at the end of the batch and the simulated distribution when the experimental seed was used as the initial condition in the model.**

Figure 12: **Comparison of experimental and simulated concentration and the simulated concentration when the experimental seed was used throughout the entire batch.**

Figure 13: Microscopic image of the a) seed distribution and b) target distribution obtained at the end of the batch.

Figure 14: Comparison of a) experimental and optimal seed distributions; b) experimental and target distributions (for which a mixture of seed was optimised) at the end of the batch, and c) experimental and simulated concentrations throughout the entire batch (for seed blend 2).

**Figure 15: Microscopic images of a) the seed distribution and b) target distribution obtained at the end of the batch (blend 2).**

**Table 1: Estimated parameters at 95% confidence interval for calibration of ATR/UV-Vis spectrometer**

| Parameter | Value | Error Bounds |
|---|---|---|
| $a_0$ | 0.0086 | $\pm 0.0002$ |
| $a_1$ | -0.6737 | $\pm 0.0025$ |
| $a_2$ | 1.7332 | $\pm 0.0013$ |
| $a_4$ | 0.0004 | $\pm 0.0001$ |

**Table 2: Process conditions for experiments for potassium dichromate-water system.**

| Process Conditions | Experiment A | Experiment B |
|---|---|---|
| Temperature profile followed | Cubic $T_{cubic} = T_0 - (T_0 - T_f)(t / t_{bacth})^3$ | Linear $T_{linear} = T_0 - (T_0 - T_f)(t / t_{batch})$ |
| Points for smooth profile, $N$ | 60 | 60 |
| Initial concentration | 0.20 g/g water | 0.20 g/g water |
| Seed loading | 1.5% of total solid | 1.5% of total solid |
| Sieve sizes for seed, $\mathcal{L}$ | 106-125µm | 106-125µm |
| Seed mass | 1.2 g | 1.2 g |
| Saturation Temperature | 30°C | 30°C |
| Initial temperature (at seeding and start of profile), $T_0$ | 29°C | 29°C |
| End temperature, $T_f$ | 20°C | 20°C |
| Sampling time for on-line measurements of CSD | 3 min | 3 min |
| Sampling time for ATR-UV/Vis and FBRM | 20 s | 20 s |
| Batch time, $t_{batch}$ | 60 min | 60 min |

**Table 3: Estimated parameters for potassium dichromate – water system considering size - dependent growth.**

| Parameter | Units | Value | Error bounds at 95% confidence interval |
|---|---|---|---|
| Growth rate constant, $(k_g)$ | $\mu m\, s^{-1}$ | 9.56 | ± 0.0832 |
| Growth constant, $(\gamma)$ | $\mu m^{-1}$ | $7.5\times10^{-3}$ | ± 0.0021 |
| Growth constant, $(p)$ | -- | 1.24 | ± 0.0633 |
| Growth order constant, $(g)$ | -- | 0.80 | ± 0.2411 |

**Table 4: Optimised seed parameters for the arbitrary target CSDs.**

| **Target CSD** | $N_G^*$ | **Selected Sieve Sizes ( $\mathcal{L}$ ) µm** | $L_{m,i}$ | $\sigma_i$ | $w_i$ |
|---|---|---|---|---|---|
| Bimodal Distribution | 5 | 37-74 | 55.5 | 18.5 | 0.08 |
| | | 74-105 | 89.5 | 15.5 | 0.21 |
| | | 105-177 | 141.0 | 36.0 | 0.03 |
| | | 177-210 | 193.5 | 16.5 | 0.24 |
| | | 210-250 | 230.0 | 20.0 | 0.44 |
| Tri-modal Distribution | 3 | 44-74 | 59 | 15.0 | 0.70 |
| | | 74-200 | 137 | 63.0 | 0.27 |
| | | 200-250 | 225 | 25.0 | 0.03 |

**Table 5: Optimised seed parameters for the arbitrary bimodal target CSDs designed for experimental investigation.**

| Simulation conditions | Seed blend 1 | Seed blend 2 |
|---|---|---|
| Target distributions, $(f_n^{tar})$ | $f_n^{tar} = 0.72\frac{1}{\sqrt{2\pi}2.40}e^{-(L-280)^2/(2.40^2)}$ $+0.28\frac{1}{\sqrt{2\pi}2.68}e^{-(L-470)^2/(2.68^2)}$ | $f_n^{tar} = 0.60\frac{1}{\sqrt{2\pi}2.18}e^{-(L-210)^2/(2.18^2)}$ $+0.40\frac{1}{\sqrt{2\pi}2.76}e^{-(L-370)^2/(2.76^2)}$ |
| Sieve fractions, (μm) | 40-63, 90-106 | 40-63, 90-125 |
| Number of Gaussians, $(N_G{}^*)$ | 2 | 2 |
| Seed mass $(m_{\text{seed}})$, (g) | 1.118 | 1.115 |
| Mean, $(L_m)$, (μm) | 51.5, 98 | 51.5, 107.5 |
| Weight fractions, $(w)$ | 0.50, 0.50 | 0.54, 0.46 |
| Standard deviations, $(\sigma)$, (μm) | 11.5, 8 | 11.5, 17.5 |

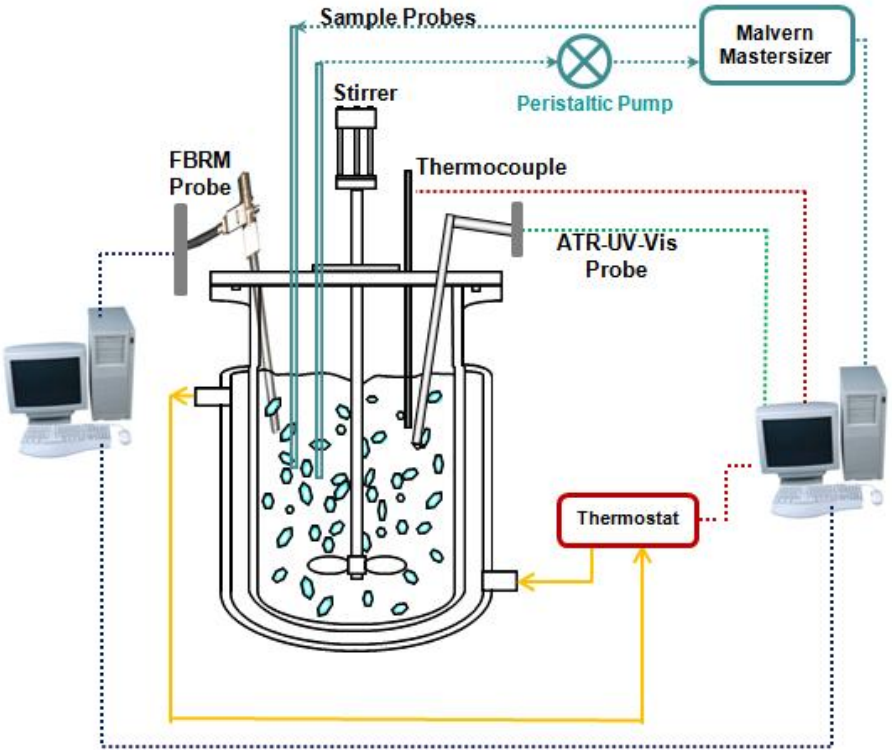


**Figure 1: A schematic representation of the experimental setup.**

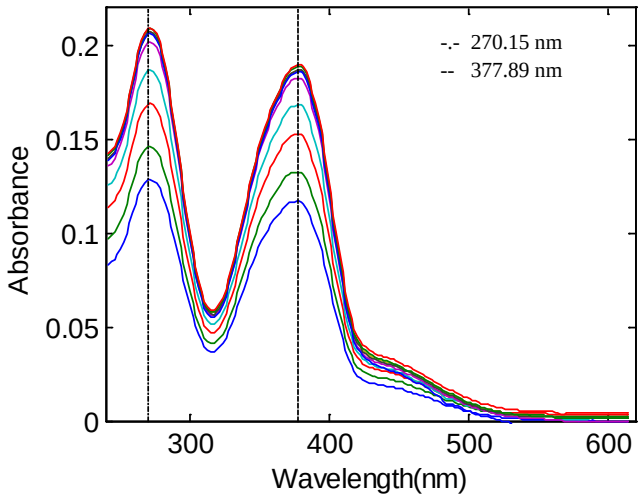


**Figure 2: UV/Vis spectra of potassium dichromate in water at different concentrations obtained using *in situ* ATR-UV/Vis spectroscopy.**

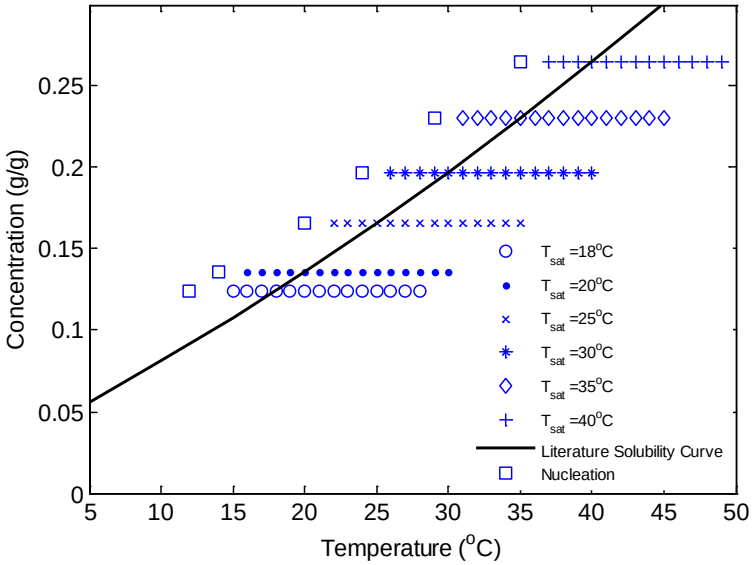


**Figure 3: Measurement points for absorbance values for the used concentrations and temperature ranges including solubility curve (Mullin, 2001) and the observed nucleation points.**

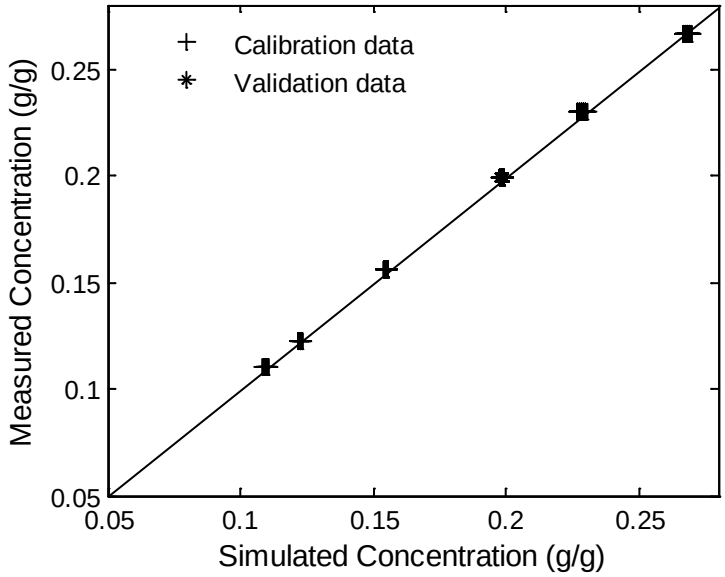


**Figure 4: Estimation and validation of calibration parameters using measured and simulated concentrations.**

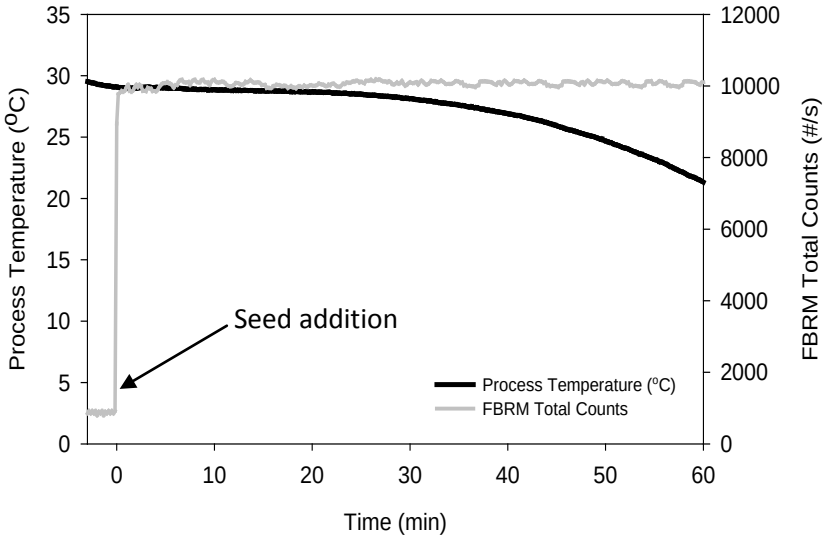


**(a)**

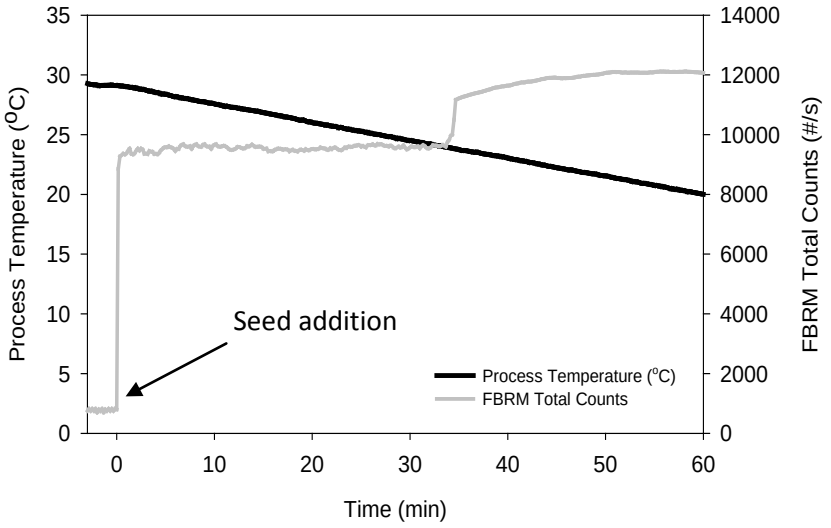


**(b)**

**Figure 5: Total counts measured by FBRM throughout the entire batch a) when the cubic profile b) when the linear profile was run for duration of 60 minutes.**

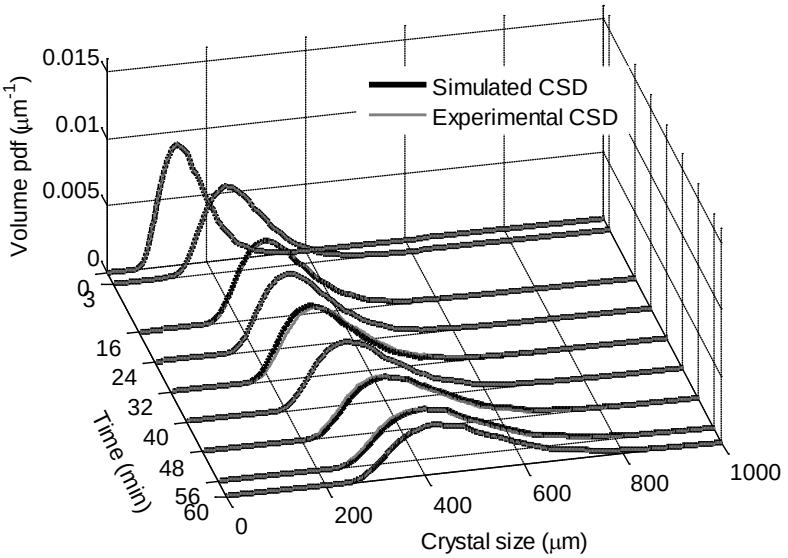


**Figure 6: Dynamic evolution of the modelled and experimental CSD for Potassium dichromate in water system for experiment A (seeded crystallisation with cubic cooling profile).**

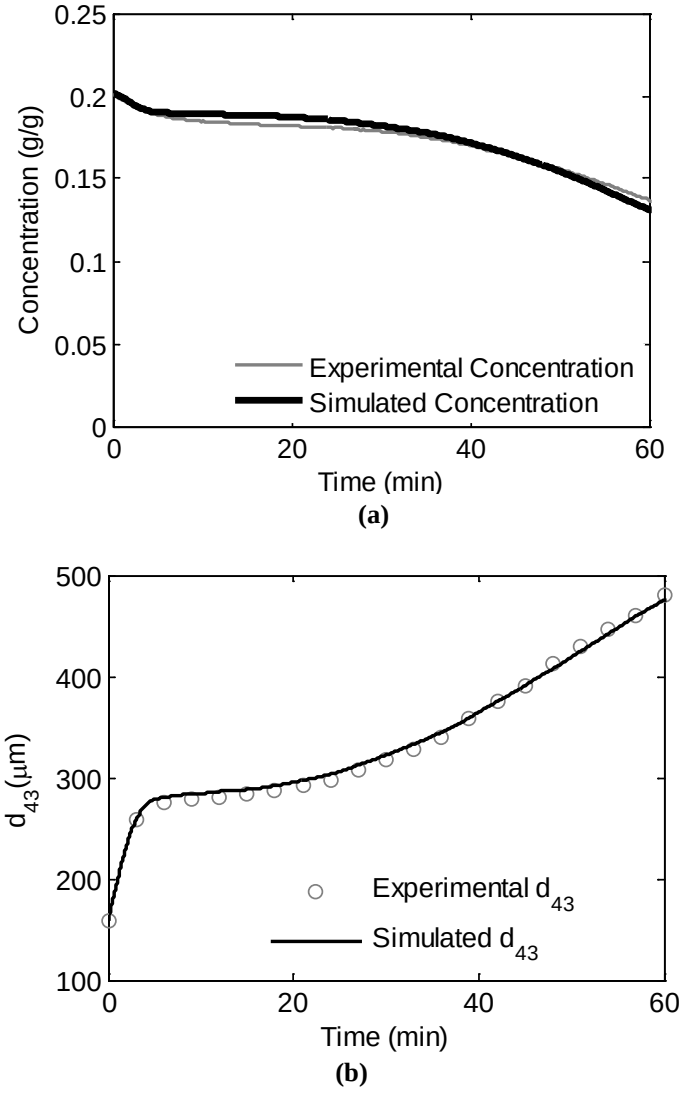


**Figure 7: Experimental and simulated results: a) concentration b) De Broucker mean diameter ($d_{43}$) during the entire batch of experiment A.**

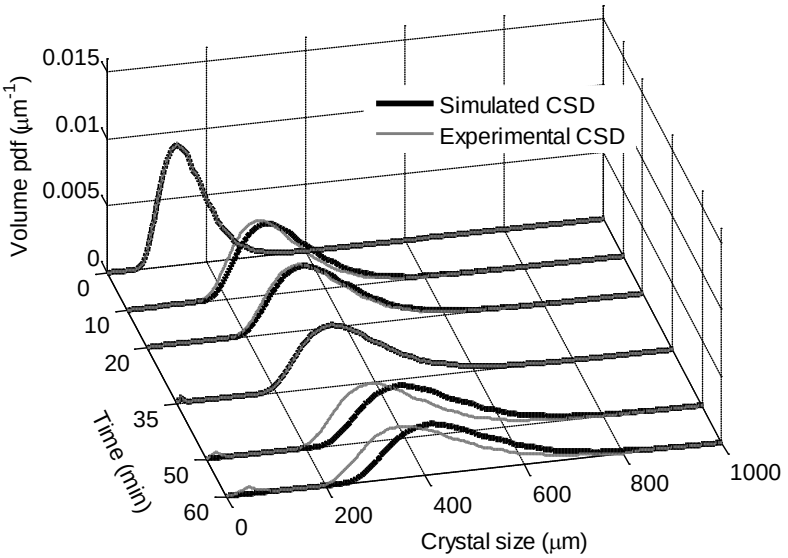


**(a)**

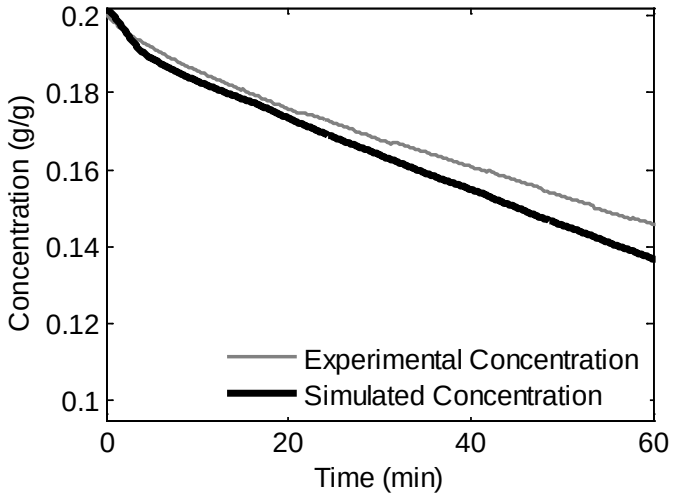


**(b)**

**Figure 8: Experimental and simulated results for experiment B to validate the modal parameters. a) Dynamic evolution of CSD and b) concentration throughout the batch for experiment B.**

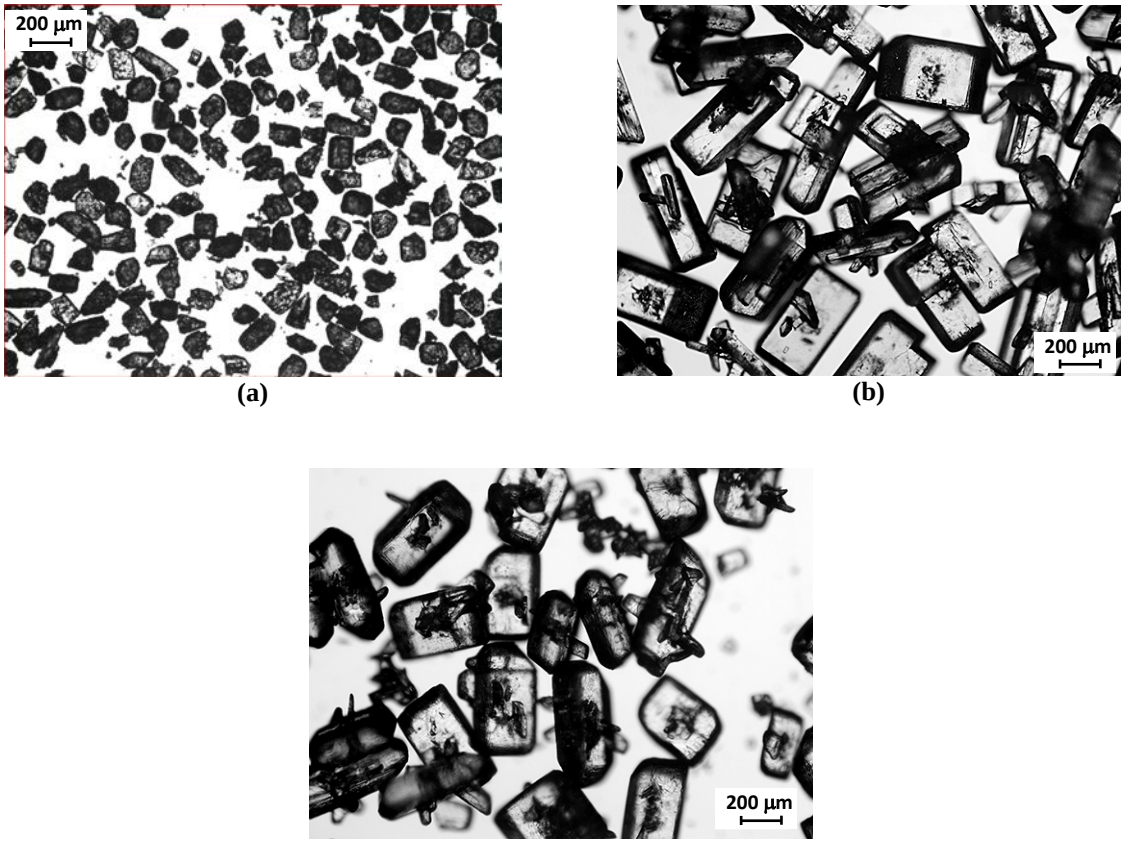


**(a)** **(b)** **(c)**

**Figure 9:** : Microscopic image of the a) seed distribution and b) crystals obtained at the end of experiment A (cubic profile) c) crystals obtained at the end of experiment B (linear profile).

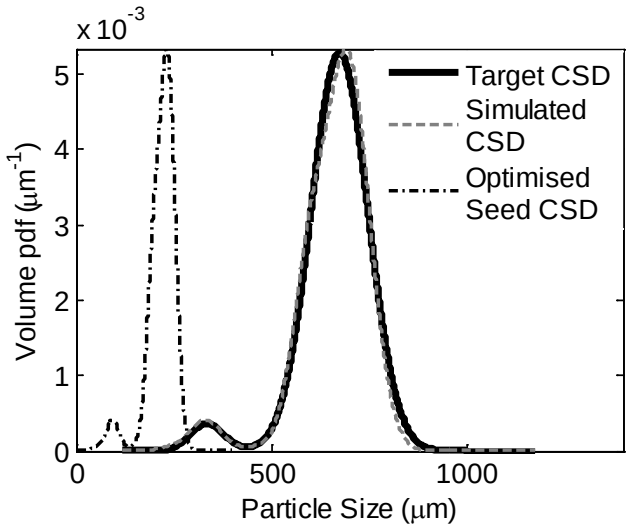


**(a)**

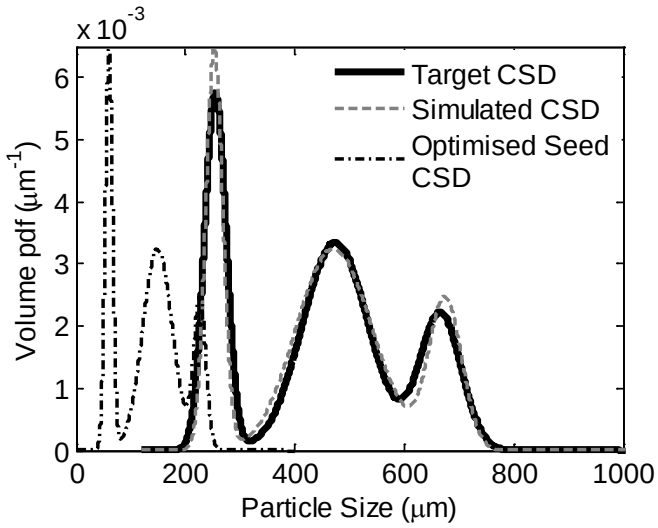


**(b)**

**Figure 10: a) Optimised seed for a bimodal target CSD; (b) optimised seed for tri-modal target CSD.**

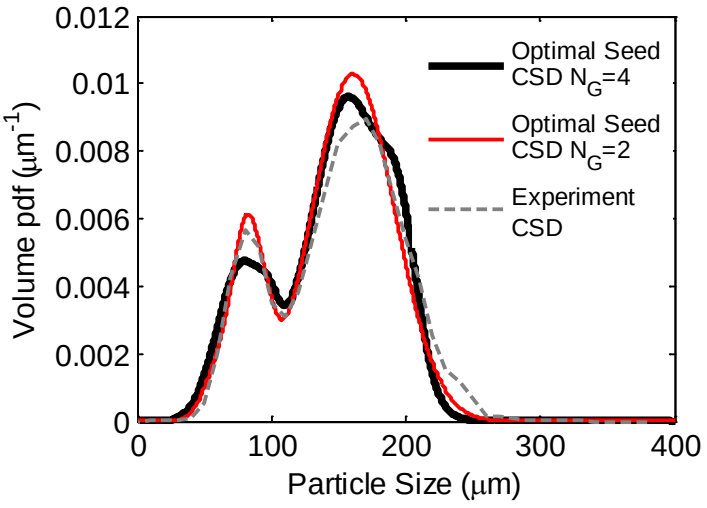


**(a)**

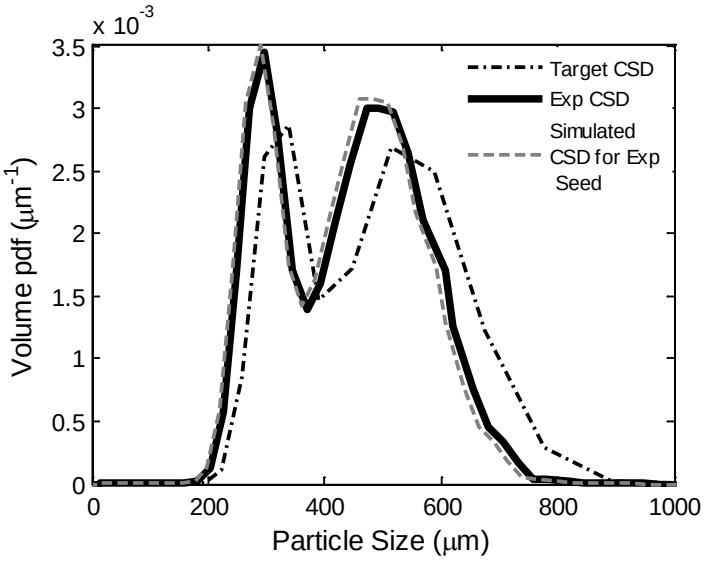


**(b)**

**Figure 11: a) Comparison of experimental and optimal seed distribution. b) Comparison of experimental and target distribution (for which a mixture of seed was optimised) at the end of the batch and the simulated distribution when the experimental seed was used as the initial condition in the model.**

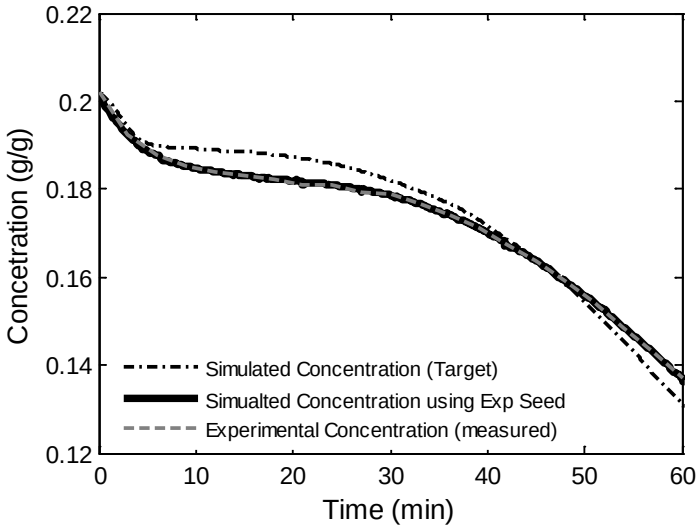


**Figure 12: Comparison of experimental and simulated concentration and the simulated concentration when the experimental seed was used throughout the entire batch.**

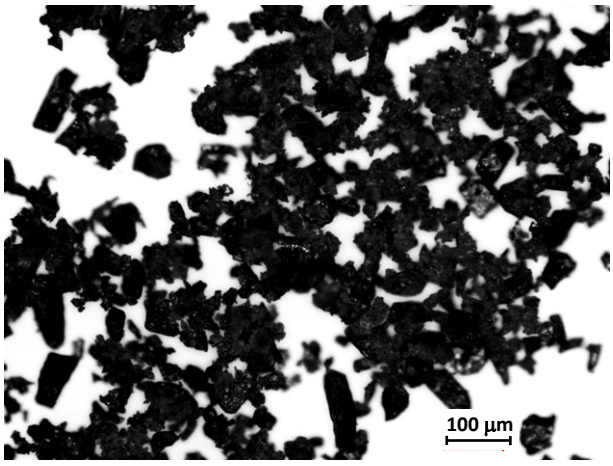


**(a)**

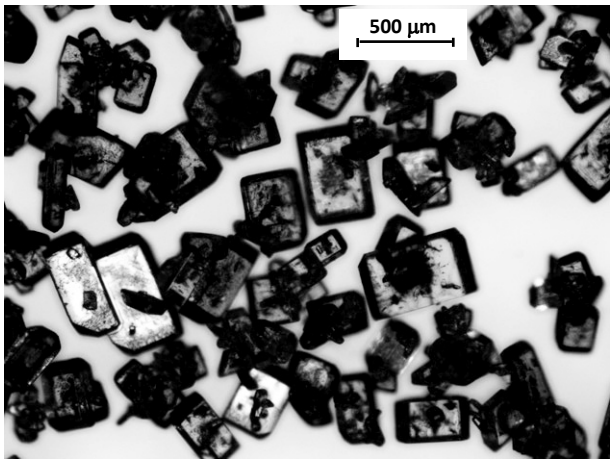


**(b)**

**Figure 13: Microscopic image of the a) seed distribution and b) target distribution obtained at the end of the batch.**

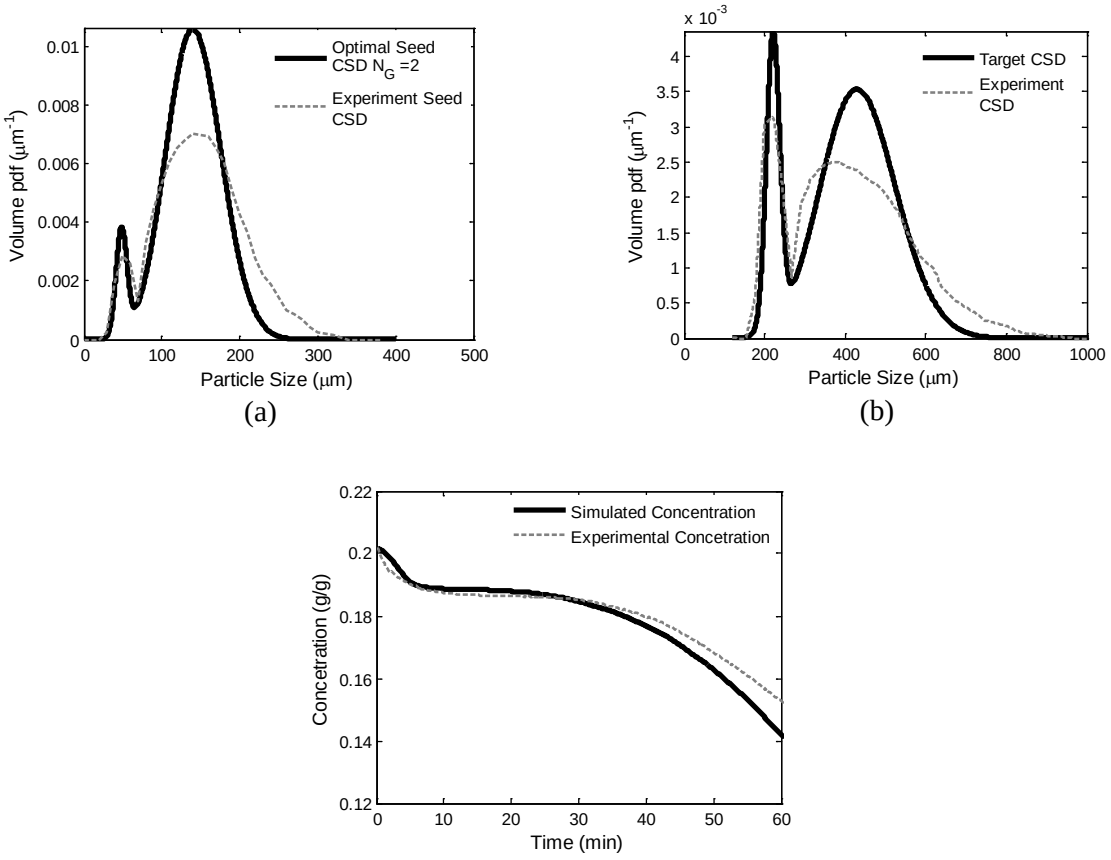


**Figure 14: Comparison of a) experimental and optimal seed distributions; b) experimental and target distributions (for which a mixture of seed was optimised) at the end of the batch, and c) experimental and simulated concentrations throughout the entire batch (for seed blend 2).**

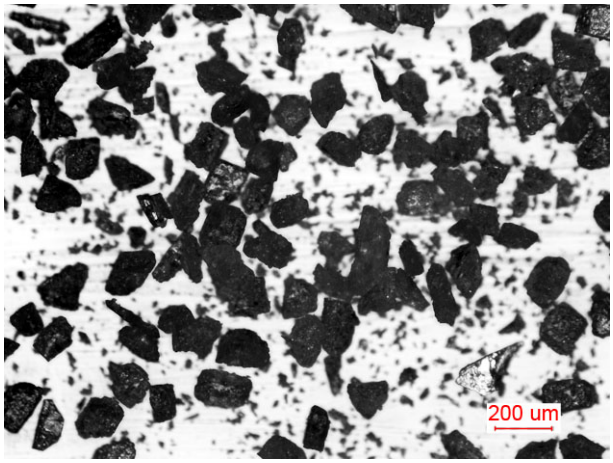


(a)

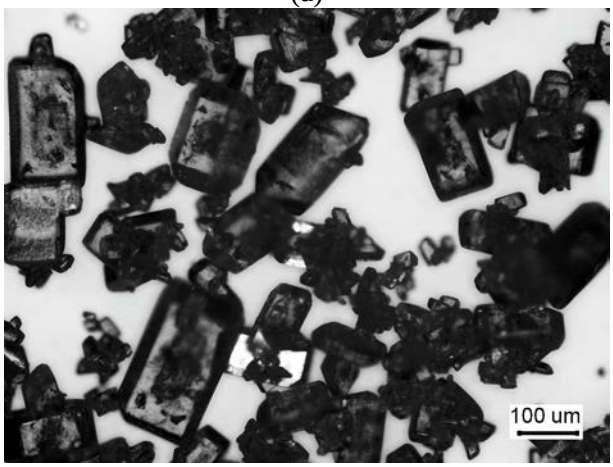


(b)

**Figure 15: Microscopic images of a) the seed distribution and b) target distribution obtained at the end of the batch (blend 2).**